Monthly Notices
of the
ROYAL ASTRONOMICAL SOCIETY

MNRAS **468,** 931–945 (2017) doi:10.1093/mnras/stx230

Impact of photometric variability on age and mass determination in young stellar objects: the case of the Orion Nebula Cluster

Sergio Messina,[1]★ Padmakar Parihar[2]★ and Elisa Distefano[1]★

[1] *INAF–Catania Astrophysical Observatory, via S. Sofia 78, I-95123 Catania, Italy*
[2] *Indian Institute of Astrophysics, Bangalore 560034, India*

Accepted 2017 January 24. Received 2017 January 10; in original form 2016 November 9

ABSTRACT

Very young stars, like the Orion Nebula Cluster (ONC) members analysed in the present study, exhibit photometric variability with a wide range of amplitudes. Such a prominent variability reflects in the inferred values of stellar colours and luminosities and, in turn, in the inferred stellar ages and masses. In this study, we measure the amplitudes of the photometric variability in *V*, *R* and *I* optical bands of a sample of 346 ONC members. We use these measurements to investigate how this variability affects the inferred masses and ages and whether it alone can account for the age spread among ONC members reported by earlier studies. We make use of colour–magnitude and Hertzprung–Russell (HR) diagrams. We find that members that show periodic and smooth photometric rotational modulation have masses and ages that are unaffected by variability when theoretical isochrones and evolutionary mass tracks are used in either colour–magnitude or HR diagrams. On the other hand, members with periodic but very scattered photometric rotational modulation and non-periodic members have masses and ages that are significantly affected. Moreover, using HR diagrams, we find that the observed *I*-band photometric variability can take account of only a fraction (∼50 per cent) of the inferred age spread, whereas the *V*-band photometric variability is large enough to mask any age spread.

Key words: stars: activity – Hertzsprung–Russell and colour–magnitude diagrams – stars: individual: Orion Nebula Cluster – stars: pre-main-sequence – stars: rotation.

1 INTRODUCTION

Almost all Orion Nebula Cluster (ONC) members are variable stars, with an amplitude of optical photometric variability ranging from a few hundredths up to more than 1 magnitude (see e.g. Herbst et al. 2002). Generally, classical T Tauri stars (CTTS) exhibit variability levels larger than weak-line T Tauri stars (WTTS: see e.g. Grankin et al. 2007, 2008; Herbst et al. 2000).

The photometric variability manifests over different time-scales, from minutes up to several years, related to different mechanisms of variability (see e.g. Messina, Rodonó & Cutispoto 2004). It manifests in all photometric bands and certainly poses difficulties if we intend to use colour–magnitude diagrams (CMDs) to infer stellar ages and masses accurately, by means of the isochronal fitting method. In fact, the uncertainties in the inferred masses and ages reflect the range of values measured in magnitudes and colours. It is worth making an effort to quantify the amplitude of variability to interpret the information inferred from the CMDs of such highly variable stars properly.

The magnitudes and colours generally observed are affected by either fading/reddening or brightening/blueing effects, due to magnetic stellar activity and variable accretion phenomena arising from star–disc interaction, and therefore they differ from the 'unspotted' values. Here, by 'unspotted' values we mean the magnitude and colours of a star, the flux of which is unperturbed by any phenomenon either in the photosphere (cool and hot spots) or in its circumstellar environment (veiling or variable disc extinction). In the following, we show that the longer the available photometric time series, the more accurate the determination of such unspotted magnitudes and colours, as well as the amplitude of variability.

Measurements of *I* magnitudes and $V - I$ colours for a substantial sample of ONC members were first carried out by Hillenbrand (1997), but from snapshot observations and, consequently, with no information on variability. Time series measurements of *I* magnitudes were subsequently made by Herbst et al. (2002, hereafter H02), who obtained repeated *I*-band observations of ONC members over an interval 45 d. Their time series allowed them to explore the range of *I*-band photometric variability with time-scales from hours to weeks. More recently, we collected five consecutive years of *I* magnitudes for a sample of 365 ONC members (Parihar et al. 2009, hereafter Paper I).

The improved accuracy we achieved in measuring the average *I* magnitudes and the amplitudes of variability with respect to the single season of H02 and the snapshot observations of Hillenbrand

★ E-mail: sergio.messina@oact.inaf.it (SM); psp@iiap.res.in (PP); eds@oact.inaf.it (ED)

Table 1. Summary of *V*-band photometry of ONC members. In column order, we list the [PMD2009] serial number, number of observations, outliers and seasons, average magnitude $V_{\rm mean}$ and its standard deviation $\sigma_{\rm tot}$ computed for the complete 5-yr time series, average seasonal standard deviation $<\sigma_{\rm seas}>$ and standard deviation of the seasonal mean magnitudes $\sigma_{<{\rm Vseas}>}$, brightest and faintest magnitude in the complete time series (see Appendix) and photometric precision. The full table is available online.

[PMD2009] number	# obs.	# out.	# season	$V_{\rm mean}$ (mag)	$\sigma_{\rm tot}$ (mag)	$\langle\sigma_{\rm seas}\rangle$ (mag)	$\sigma_{\langle{\rm Vseas}\rangle}$ (mag)	$V_{\rm min}$ (mag)	$V_{\rm max}$ (mag)	Precision (mag)
1	1	0	1	19.037	0.0	0.0	0.0	0.0	0.0	0.841
2	16	0	1	19.205	0.48	0.464	0.255	19.455	18.714	0.091
3	60	0	3	17.868	0.13	0.101	0.019	18.123	17.617	0.039
4	112	0	4	16.367	0.113	0.072	0.027	16.541	16.166	0.02
5	231	0	4	16.242	0.253	0.196	0.071	16.678	15.858	0.043
...	...	...	...	...	...	...	...	...	...	...

Table 2. Summary of *I*-band photometry of ONC members. The full table is available online.

[PDM2009] number	# obs.	# out.	# season	$V_{\rm mean}$ (mag)	$\sigma_{\rm tot}$ (mag)	$\langle\sigma_{\rm seas}\rangle$ (mag)	$\sigma_{\langle{\rm Vseas}\rangle}$ (mag)	$V_{\rm min}$ (mag)	$V_{\rm max}$ (mag)	Precision (mag)
1	334	2	4	13.944	0.126	0.099	0.04	14.283	13.794	0.026
2	238	0	5	17.545	0.383	0.322	0.067	18.272	16.822	0.052
3	320	0	5	15.004	0.038	0.035	0.01	15.065	14.931	0.017
4	310	0	5	13.421	0.079	0.044	0.013	13.586	13.293	0.011
5	558	3	5	14.318	0.207	0.19	0.081	15.078	13.972	0.029
...	...	...	...	...	...	...	...	...	...	...

(1997) is evident in fig. 5 of Paper I. The snapshot observations of Hillenbrand for numerous common stars differ by up to two magnitudes from our mean *I* magnitudes, whereas those of H02 never differ by more than one magnitude.

It is true that Herbst and collaborators have been monitoring ONC at Van Vleck Observatory (Herbst et al. 2000) in the *I* band since 1991, i.e. for a time interval much longer than ours, deriving average magnitudes and variability amplitudes more accurately than us and for a larger sample of stars. The major improvement that we obtained is that we measured the magnitudes in contemporary fashion in three different bands (*V*, *R* and *I*) and for 5 consecutive years. This puts us in a better position to derive average values to position ONC stars in CMDs and to investigate what impact the photometric variability may have on age and mass determination.

We present the data in Section 2 and our analysis in Section 3. The effects of rotation and long-term cycles on observed magnitudes and colours are presented in Section 4. The modelling of colour variations is presented in Section 5 and, finally, a discussion and conclusions are presented in Sections 6 and 7.

2 DATA

As described in Paper I, we have collected five seasons (from 2003–2004 to 2007–2008) of *I*- and *V*-band data and one season (2007–2008) of additional *R*-band data for a total of 346 ONC members. To date, this is the most complete (in terms of the number of photometric bands) multi-year data base of *VRI* observations for ONC members.

Our members belong to a 10×10 arcmin^2 field of view (FoV) located south-west of the Trapezium stars and with extinction-corrected magnitudes and colours in the range $12 \lesssim V_0 \lesssim 20$ mag and $0 \lesssim (V-I)_0 \lesssim 5$ mag, respectively. Starting from the 2008–2009 season, we have been monitoring a larger 20×20 arcmin^2 region to make our data base more complete in terms of members.

Our stellar sample has been observed with the 2-m Himalayan Chandra Telescope (HCT) and the 2.3-m Vainu Bappu Telescope (VBT) of the Indian Astronomical Observatory (IAO, India). On each telescope pointing, we collected 3–4 consecutive frames within very short intervals of time (<1 h) that were subsequently combined to compute an average magnitude value and its standard deviation, which we use as a robust estimate of the photometric accuracy achieved. In the following, we intend for observation the average of the above-mentioned 3–4 consecutive observations. More of such telescope pointings were made during each observation night. We refer the reader to Paper I for a detailed description of the observation strategy, pre-reduction process, magnitude extraction and data preparation.

Briefly, in order to remove possible outliers from our data time series, we applied a 3σ clipping filter. Owing to the season-to-season variation of the star's average magnitude, it turned out to be more accurate to apply such a filter to each seasonal time series rather than to the whole time series. The observation season generally lasted 2–6 consecutive months. In such a way, about 0.15 per cent of observations were discarded for the subsequent analysis. A fraction of such outliers may arise from intrinsic variability, likely related to flare events.

In Tables 1–3 we summarize the photometric properties of our targets in the *V* and *I* bands and in $V-I$ colour, respectively. In column order, we list the [PMD2009] serial number, number of observations, outliers and seasons, average magnitude $V_{\rm mean}$ and its standard deviation $\sigma_{\rm tot}$ computed for the complete 5-yr time series, average seasonal standard deviation $<\sigma_{\rm seas}>$ and standard deviation of the seasonal mean magnitudes $\sigma_{<{\rm Vseas}>}$, brightest and faintest magnitude in the complete time series and photometric precision. We refer the reader to the Appendix for a description of the method used to measure the brightest/faintest magnitudes and the amplitude of variability. To make a more accurate estimate of these quantities, we considered only seasons with at least 10 observations for each star.

Table 3. Summary of $V - I$ photometry of ONC members. The full table is available online.

[PDM2009] number	# obs.	# out.	# season	V_{mean} (mag)	σ_{tot} (mag)	$\langle\sigma_{seas}\rangle$ (mag)	$\sigma_{\langle Vseas\rangle}$ (mag)	V_{min} (mag)	V_{max} (mag)	Precision (mag)
1	2	0	0	5.041	0.0	0.0	0.0	5.041	5.041	0.841
2	36	0	1	1.968	0.532	0.0	0.0	3.109	0.891	0.095
3	66	0	3	2.875	0.126	0.0	0.0	3.136	2.591	0.041
4	98	0	4	2.932	0.158	0.0	0.0	3.162	2.673	0.022
5	213	0	4	1.872	0.29	0.0	0.0	2.239	1.125	0.05
...	...	...	...	...	...	...	...	...	...	...

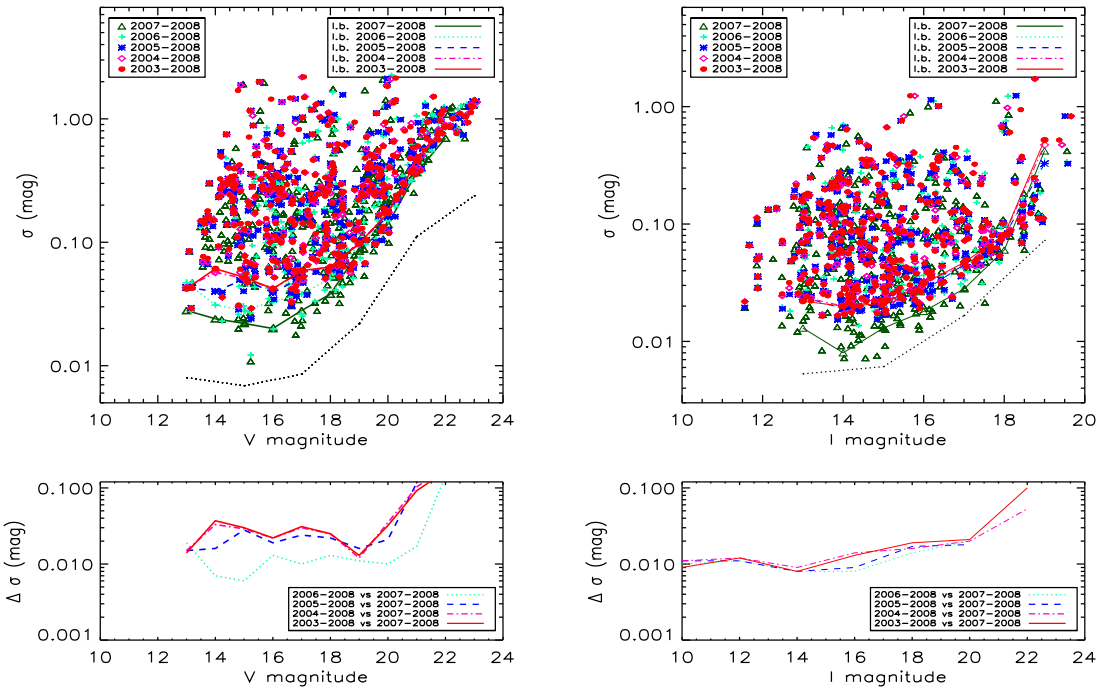

Figure 1. Top panels: standard deviation (σ) versus mean magnitude (left for V band and right for I band) for the complete sample of ONC members computed considering time intervals of increasing length. The lines represent the corresponding lower envelopes of the σ distributions. The lowest dotted line represents the photometric precision. Bottom panels: differences between the lower envelopes computed considering time intervals of increasing length with respect to the last observation season.

3 CAUSES OF VARIABILITY

The photometric variability of low-mass pre-main-sequence and main-sequence stars arises from a number of phenomena[1] that manifest on different time-scales (see e.g. Messina et al. 2004). The phenomenon that produces the most stable and best characterized variability is the rotational modulation of surface inhomogeneities. Its time-scale (i.e. the rotation period) ranges from about half a day to several days and, generally, is never longer than about 20–30 d.

Another contribution to the observed variability, the amplitude of which can be larger than that arising from rotational modulation, comes from transient phenomena like flares or extinction-related brightness fadings and manifests on shorter time-scales. Owing to its stochastic nature, it is less easily characterized.

Active region growth and decay (ARGD), variable accretion and activity cycles also contribute to the photometric variability on the longest time-scales, from several weeks for the former to several years for the latter. Their characterization requires multi-year monitoring.

Each cause of variability has a spectrum of amplitudes, the range of which can be accurately determined if the photometric time series is much longer than the respective time-scales, i.e. if the same phenomenon producing the variability is sampled several times by observations.

In our study, we can state that our 5-yr long monitoring is suited to characterizing the amplitude of variability arising from both rotational modulation and ARGD. On the other hand, an observational sampling more frequent and uninterrupted than ours is required to gather robust statistics of stochastic phenomena, which is beyond our range of possibilities. Our monitoring has allowed us to detect these phenomena, but certainly not their complete amplitude spectrum. Finally, starspot cycles and long-term trends exhibit time-scales of variability longer than 5 yr and up to decades. Therefore, we can derive only lower limits on their amplitudes.

As a matter of fact, the longer the time series, the better the characterization of the whole spectrum of variability.

In Fig. 1, we show, as an example for the V and I bands, how the level of observed variability and therefore the capability of

[1] In our analysis of variability phenomena, we limit ourselves to single stars and non-eclipsing binaries.

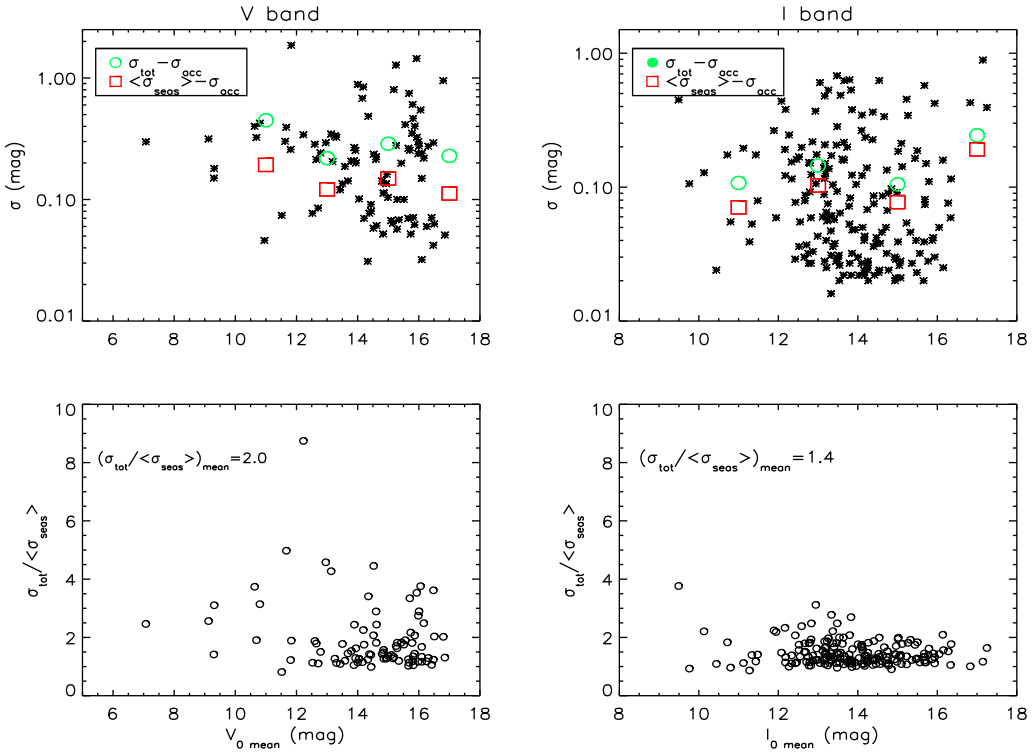

Figure 2. Top panels: total standard deviation $\sigma_{\rm tot}$ (asterisks) versus reddening-corrected mean magnitude for V (left) and I band (right). Open circles and squares represent the average values, computed within bins of 2-mag width, of $\sigma_{\rm tot}$ and $<\sigma_{\rm seas}>$, both corrected for the photometric precision $\sigma_{\rm acc}$. Bottom panels: ratio between $\sigma_{\rm tot}$ and $<\sigma_{\rm seas}>$ versus reddening-corrected mean magnitude.

detecting the complete amplitude spectrum increases as the time series lengthens.

We display for each target the V-band (left) and I-band (right) standard deviation versus mean magnitude considering the last observation season to begin, i.e. observations collected in 2007–2008 (green triangles), which is our longest observation season, and overplot its lower envelope (green solid line). This envelope is computed by averaging the 10 per cent smallest values within each bin of one magnitude width. Then, we consider the standard deviation from the last two years of observations (sky-blue crosses) and so on. Finally, we consider the $\sigma_{\rm tot}$ (red bullets) of the complete time series.

It is evident that, as the series becomes longer, the variability amplitude, as measured by the standard deviation, tends to increase. This happens because we are obtaining a more accurate estimation of all variability components. As shown in the lower panels of Fig. 1, the largest increase is obtained when we add a second consecutive season of observations and again a third. Starting from the fourth consecutive season, the lower envelope continues to increase, but at a much smaller rate. In the case of the I-band observations, we see a similar behaviour, although the variability in the I band is smaller than that in the V band and the standard deviation lower envelope increases less rapidly than in the V-band case.

We find that ONC members exhibit a photometric variability, the average seasonal standard deviation of which, corrected for photometric accuracy (dotted black lines in the top panels of Fig. 1), is $<\sigma_{{\rm seas}\_V}> = 0.24$ mag and $<\sigma_{{\rm seas}\_I}> = 0.12$ mag, whereas the total standard deviation (on a 5-yr base line) is $<\sigma_{{\rm tot}\_V}> = 0.39$ mag and $<\sigma_{{\rm tot}\_I}> = 0.17$ mag.

This first result is in agreement with the well-known dependence of variability amplitude on wavelength. The use of I-band photometry allows us to deal with a photometric variability smaller with respect to V-band photometry (in our case smaller by a factor of 2) and is preferable in positioning ONC members in CMDs.

To investigate any dependence of the variability level on stellar mass, we have to correct our mean magnitudes for interstellar extinction. Unfortunately, we have values of extinction ($A_{\rm v}$) for only about 25 per cent of our sample, specifically only for the brighter members. Using the Hillenbrand (1997) $A_{\rm v}$ values (see Section 3.3) to correct the magnitudes for reddening, we find that the average variability levels are $<\sigma_{{\rm tot}\_V}> = 0.24$ mag and $<\sigma_{{\rm seas}\_V}> = 0.12$ mag ($<\sigma_{{\rm tot}\_I}> = 0.12$ mag and $<\sigma_{{\rm seas}\_I}> = 0.09$ mag) in the $10 < V_0 < 15$ mag range (i.e. stars with $M > 0.3$–0.4 M$_\odot$).

We plot these results in the top panels of Fig. 2, using asterisks to represent $\sigma_{\rm tot}$ and open bullets and squares to represent the average values of $\sigma_{\rm tot}$ and $<\sigma_{\rm seas}>$ (obtained using a binning width of 2 mag). In the bottom panels of Fig. 2, we plot the ratio of these quantities versus magnitude. We find that the average ratios are 2.0 and 1.4 for the V and I bands, respectively, and no significant dependence on mass is found.

In the following subsections, we show that when we consider the contribution to variability arising only from periodic phenomena, i.e. the light rotational modulation due to dark/hot spots, then its impact on mass and age estimation is negligible. On the other hand, when we consider the additional contribution of other non-periodic phenomena, e.g. related to variable accretion or ARGD, then the impact of variability becomes increasingly significant.

The best approach to disentangle the contribution to variability by spot rotational modulation from the others is to analyse periodic and non-periodic variables separately, as will be discussed in the following.

3.1 Samples of 'clean' and 'dirty' light curves

One major difficulty in estimating the amplitude of rotation-induced variability from data time series is the presence of possible outliers, which can return incorrect average values, but more critically incorrect brightest and faintest values, thus overestimating the amplitude of variability. The contribution of ARGD and activity cycles is minimized by segmenting the 5-yr long time series into segments each corresponding to the yearly observation season.

Periodic variables are best suited to identifying and removing outliers, allowing us to measure the correct amplitude of rotation-induced variability more confidently. In fact, once the data time series of periodic stars are phased into folded light curves, it becomes quite easy to identify any data that deviate significantly from the trend imposed by the rotational modulation. These outliers can arise either from bad measurements or from the above-mentioned transient phenomena, which are likely unrelated to the rotational modulation.

We know the rotation periods of 165 of the 346 stars considered in the present analysis. The rotation periods of 55 stars were discovered by us (Paper I) and those of another 17 stars by Rodriguez-Ledesma, Mundt & Eisloeffel (2009), whereas the remaining 93 stars had a period already known in the literature (e.g. Herbst et al. 2000, 2002; Stassun et al. 1999).

We have produced phased light curves of all 165 periodic stars. Then, we have automatically removed from each light curve all data deviating more than 3σ from the mean value and any other remaining observation that, with visual inspection, appeared to deviate significantly from the sinusoidal trend imposed by the rotational modulation.

After cleaning the phased light curves from outliers, we have selected a subsample consisting of very smooth light curves. These are light curves that were best fitted by a single sinusoidal function and for which the ratio (R) between the amplitude and the average residuals from the fit was arbitrarily set to be $R \geq 2.5$. Since these smooth light curves also exhibit some level of magnitude dispersion at any given rotation phase, in the following we adopt the brightest and faintest values of the sinusoidal fit as the brightest and faintest light-curve values. In Fig. 3, we give an example of the analysis we carried out for each periodic star in each observation season. In this specific example, we consider the star [PMD2009] 311, the light curves of which in the 2007–2008 season are all very smooth. The top left panels display the I, R and V magnitudes and the top right panels display the $V-I$, $R-I$ and $V-R$ colour curves phased with the rotation period $P = 9.89$ d taken from Paper I. The solid blue lines are the sinusoidal fits to the data with the rotation period. In the bottom panels we plot the magnitude versus colour and colour versus colour distributions, which are linearly fitted (red solid line) and for which the Pearson linear correlation coefficients and significance levels are computed. The slopes of these relations, computed from regression analysis, provide valuable information on the average temperature contrast of the surface inhomogeneities with respect to the unperturbed photosphere. These slopes can change from star to star and, for the same star, can change from season to season.

Using the R value as a criterion to distinguish light curves, we were left with one subsample of very smooth light curves (hereafter named 'clean' periodic) with $R \geq 2.5$ and one subsample of quite

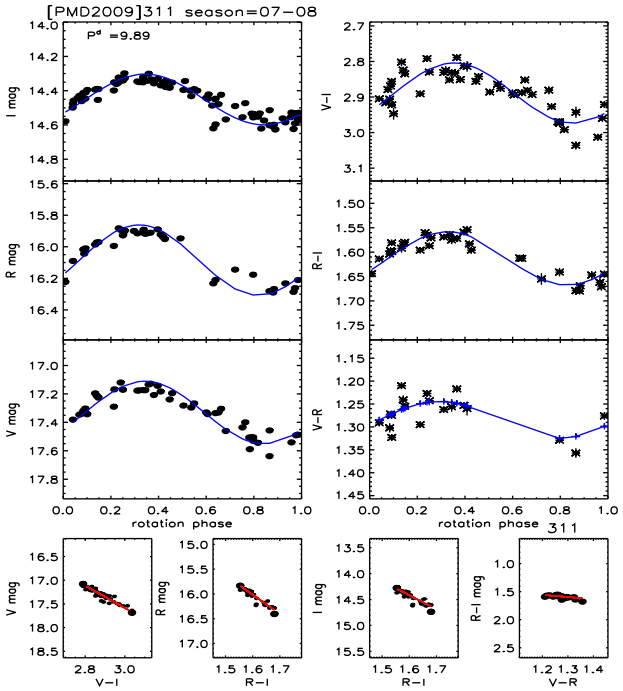

Figure 3. Example of 'clean' magnitude and colour curves (top panels) of the star [PMD2009] 311 in the season 2007–2008. Data are folded with the rotation period and fitted with a single sinusoidal function (solid line). The magnitude versus colour and colour versus colour distributions are plotted in the botton panels, together with a linear fit (solid line).

scattered light curves (hereafter named 'dirty' periodic) with $1.0 \leq R < 2.5$. Stars with $R < 1$, although their rotation period is known from the literature, show no light rotational modulation in our time series.

We remind the reader that each periodic star has up to five light curves in the I band and up to five in the V band (since the complete time series is analysed after splitting into five consecutive seasons), whereas it has only one light curve in the R band, which is available for the 2007–2008 season. We find that each star during the same season can have either all light curves (V, I, $V-I$) clean or all dirty, or a combination, and that circumstance can change from season to season.

In general, dirty light curves are more numerous than clean ones. For a total of 797 I-band light curves, 45 per cent are clean; for a total of 156 R-band light curves, 26 per cent are clean; for a total of 800 V-band light curves, 31 per cent are clean. If we consider that about 50 per cent of the complete stellar sample (346 stars) is made up of non-periodic stars (the time series of which can be considered as dirty), then we find that, among ONC members, clean light curves are found with a percentage never larger than 25 per cent in the I band and never larger than 15 per cent in the V band. As extreme cases, we mention the following stars: [PMD2009] 57, 147, 182, 191, 256, 274, 311, 333, the light curves of which are all and always clean, whereas the stars [PMD2009] 23, 98, 100, 132, 185, 192, 224, 227, 334, 337 all and always have dirty light curves.

In Fig. 4, we plot the normalized distributions of the magnitude and colour curves amplitudes for the 'clean' sample on a logarithmic scale. Labels report the number of light curves (l.c.) used to build the distributions and the average peak-to-peak light-curve amplitude. On average, the V light curves have amplitudes larger than R and I light curves and the $V-I$ colour curves have amplitudes larger than $V-R$ and $R-I$. Such a trend is consistent with variability

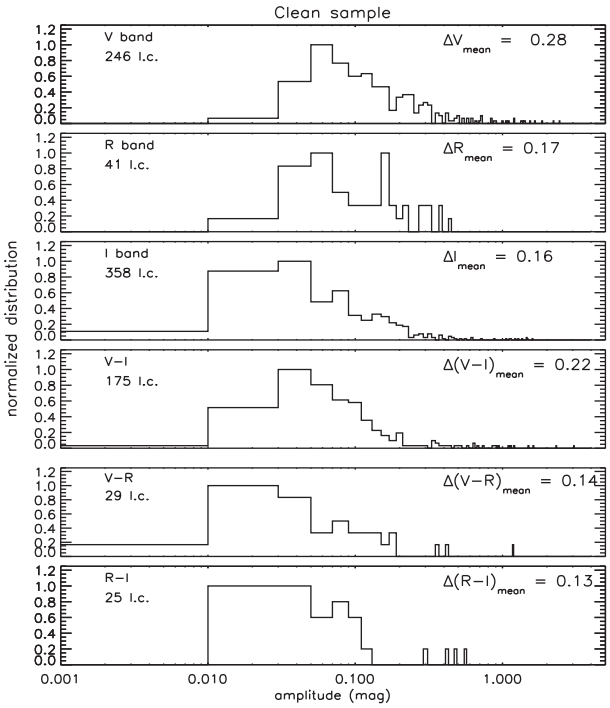

Figure 4. Normalized distributions of light and colour curve amplitudes from the clean sample. Labels indicate the number of curves (l.c.) used to build the distributions.

arising from temperature inhomogeneities (either hotter or cooler than the unperturbed photosphere) carried in and out of view by the stellar rotation. Generally, among pre-main-sequence weak-line T Tauri stars or main-sequence stars, whose photometric variability is dominated by cool spots, amplitudes are not larger than 0.5 mag (see e.g. Messina, Rodonó & Guinan 2001, Messina et al. 2010, 2011). Nonetheless, exceptions exists, like the T Tauri star V410 Tau for which light curve amplitudes up to $\Delta V = 0.7$ mag are been measured (e.g. Oáh et al. 2009). Our detection of larger amplitudes in a few stars then may suggest that also hot spots on the stellar photosphere created by disk accretion may be present in our clean star sample.

3.2 CMD for 'clean' periodic light curves

To compare our observations with theoretical isochrones in CMDs, we have to remove the effect of reddening from our measurements. We have at our disposal the works by Hillenbrand (1997) and, more recently, Da Rio et al. (2010), in which the reddening of numerous ONC members is computed. In the first work, we find measured reddening A_V for 108 out of 165 periodic stars, in the second case for 97 out of 165. Hillenbrand (1997) and Da Rio et al. (2010) use different methods to estimate A_V and, for our periodic stars in common to both studies, their estimates differ on average by $A_{V\_Hill} - A_{V\_DaRio} = -0.93$ mag (with differences ranging from −3.9 mag to 1.3 mag). In the following analysis, we use only a subsample of 'clean' light curves with known extinction to build our CMDs, whereas to investigate the slopes of the magnitude versus colour variations (which are independent of extinction) we can use the complete sample. To preserve homogeneity, we make use only of the Hillenbrand A_V determinations, which allow us to consider a more numerous sample of extinction-corrected light curves.

In the left panel of Fig. 5, we plot, in the form of segments, the intrinsic V_0 magnitude and $(V - I)_0$ colour variations derived from the clean sample of light curves. We find that all V_0 versus $(V - I)_0$ variations have correlation coefficients with significance levels larger than 95 per cent. We use black, red and green colours to distinguish V_0 versus $(V - I)_0$ variations with correlation coefficient $r > 0.95$, $0.90 < r < 0.95$ and $r < 0.90$, respectively. For instance, two or

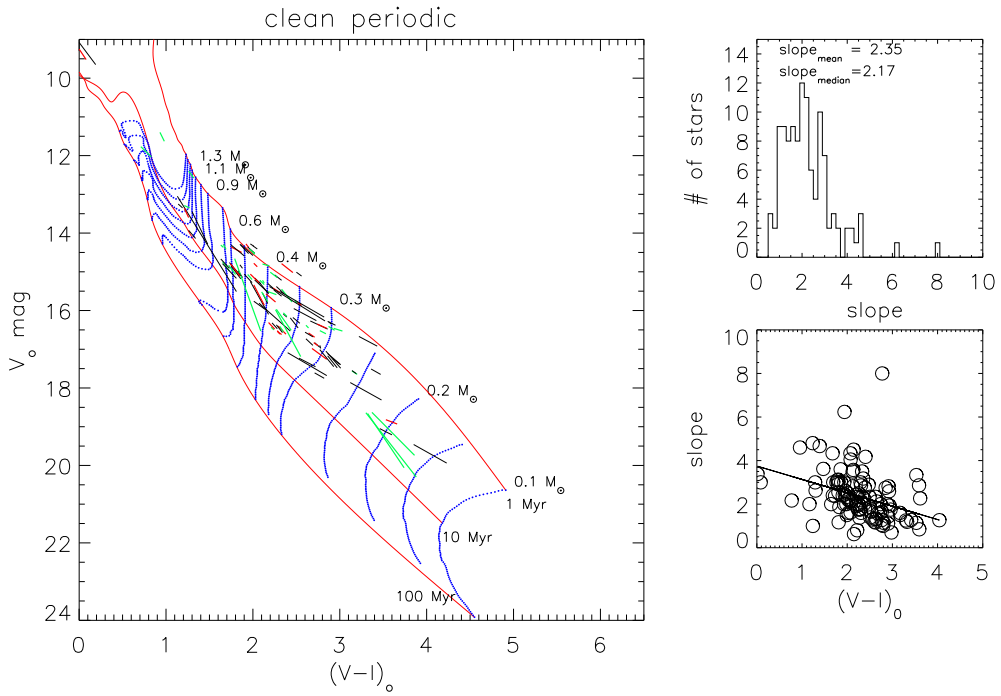

Figure 5. Left panel: V_0 versus $(V - I)_0$ diagram for the sample of 'clean' light curves. Red solid lines and blue dotted lines represent theoretical isochrones and mass tracks, respectively, from Siess et al. (2000). Black and grey segments indicate different degrees of correlation ($r > 0.95$ and $r < 0.95$, respectively). Top right panel: distribution of slope of V_0 versus $(V - I)_0$ variations; bottom right panel: distribution of slope versus $(V - I)_0$ colour.

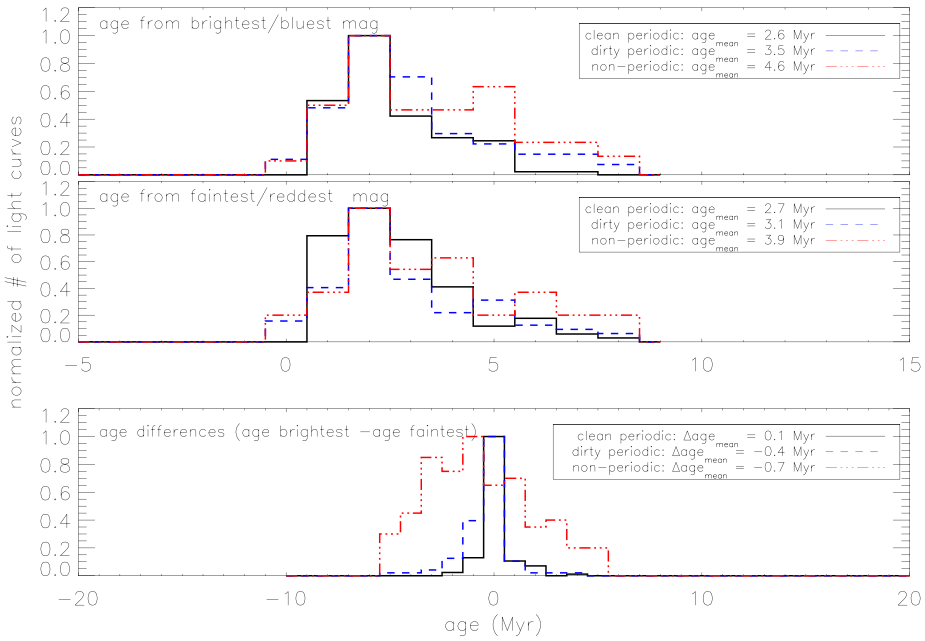

Figure 6. Distribution of ages for ONC members for 'clean' periodic (solid line), 'dirty' periodic (dashed line) and non-periodic (dot–dashed line) cases, derived from the brightest/bluest magnitude (top panel), faintest/reddest magnitude (middle panel) and their difference (bottom panel).

more segments may refer to the same star, but corresponding to different seasons. We overplot the isochrones for 0.1, 1 and 10 Myr and the zero-age main sequence (ZAMS, solid red lines) computed according to the Siess, Dufour & Forestini (2000) models for solar metallicity. We also plot the evolutionary mass tracks (dotted blue lines) for different mass values in the range 0.1–1.5 $M_{\odot}$.

The slopes $\Delta V_0/\Delta(V-I)_0$ exhibit a range of values, the mean and median of which are 2.35 and 2.17, respectively (see top right panel). Moreover, the slopes appear to decrease with increasing colour (decreasing mass). We found similar results when data are analysed separately, according to the correlation coefficient values ($r > 0.95$, $0.90 < r < 0.95$ and $r < 0.90$).

A comparison with a family of isochrones from Siess et al. (2000) (at steps of 1 Myr) allows us to estimate the age of our targets. Specifically, we infer two different ages from each light curve, one corresponding to the light-curve brightest/bluest value and another to the faintest/reddest value. The difference between the two inferred ages provides us with an estimate of the impact of variability, arising from rotational modulation of spots, on the age estimate of that star within the same observation season. Since, from season to season, the position of the targets (represented by a segment in the CMD) can change owing to AR evolution, our results represent only the effects of rotational modulation. A visual inspection clearly shows that, on average, the presence of surface inhomogeneities on the stellar surface induces magnitude and colour variations with slope similar to that of the isochrones in the CMD. This means that the impact on age determination is not significant. Nonetheless, we can compute the age of our stars and the results are plotted in the panels of Fig. 6. Here, we plot using solid lines the distribution of ages derived from brightest/bluest values (top panel), from faintest/reddest values (middle panel) and their differences, i.e. ages from faintest minus ages from brightest (bottom panel). We find that the highest and lowest mean ages are about the same (2.7 and 2.6 Myr, respectively); also, the average age difference of 0.1 Myr is not significant. Nonetheless, we found 10 per cent of cases for which the activity-induced apparent age difference is larger than 1 Myr (up to 8 Myr). We stress that our aim is not to compute an absolute age of the ONC members, rather to estimate the age dependence on photometric variability. This is the reason that our analysis did not need to use different evolutionary models.

Similarly, we can derive the mass of our targets by comparison with a family of mass evolutionary tracks (at steps of 0.1 $M_{\odot}$). Again, we derive two mass values for each light curve, corresponding to the brightest/bluest and the faintest/reddest values. The results are plotted in Fig. 7. Here, we show using solid lines the distribution of masses derived from brightest/bluest (top panel), faintest/reddest (middle panel) and their difference (bottom panel), the mean values of which are 0.46 $M_{\odot}$, 0.50 $M_{\odot}$ and 0.04 $M_{\odot}$, respectively. Again, these differences are smaller than the precision associated with our mass determination (i.e. the 0.1-$M_{\odot}$ step). Nonetheless, in about 4 per cent of cases the mass difference is larger than 0.1 $M_{\odot}$. We note in Fig. 5 that the sensibility of mass versus $V-I$ colour variations decreases as we move towards lower masses: a mass difference of 0.1 $M_{\odot}$ is accompanied by a colour variation of $\Delta(V-I) = 0.01$ mag at $M = 1$ $M_{\odot}$ and $\Delta(V-I) = 0.1$ mag at about $M = 0.2$ $M_{\odot}$. Therefore, although the bottom right region of the CMD is populated by longer segments, the corresponding mass variation is not longer at all.

We have carried out a similar analysis (see Fig. 8) for the intrinsic I_0 versus $(V-I)_0$ variations and obtained, as expected, the same results. Also in this case, the activity-induced apparent age differences derived in 10 per cent of light curves are larger than 1 Myr (up to 4 Myr; up to 20 Myr in only one case).

We conclude that, if all ONC members were periodic variable and all light curves smooth, then the impact of photometric variability on the average determination of age would be negligible and CMDs would be well suited to infer both mass and age. Only a fraction (10 per cent) of stars may have their age and mass significantly affected by photometric variability. However, as already mentioned, only 50 per cent of ONC stars in our small sample are periodic and in total only 25 per cent have smooth light curves. Therefore, it is important to see what role the variability plays in the remaining targets.

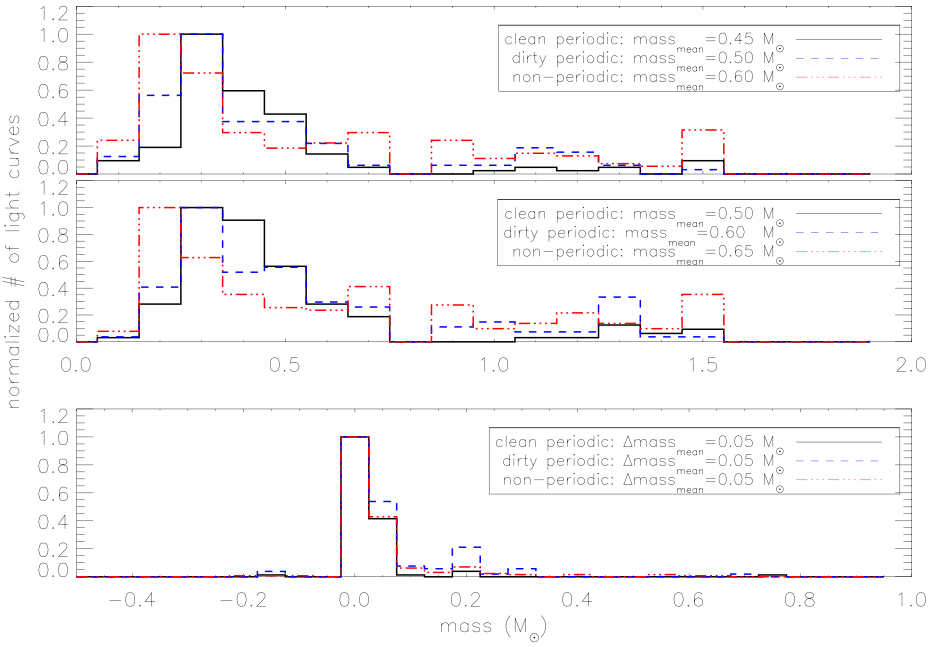

Figure 7. Distribution of masses for ONC members for 'clean' period (solid line), 'dirty' periodic (dashed line) and non-periodic (dot–dashed line) cases, derived from the brightest/bluest magnitude (top panel), faintest/reddest magnitude (middle panel) and their difference (bottom panel).

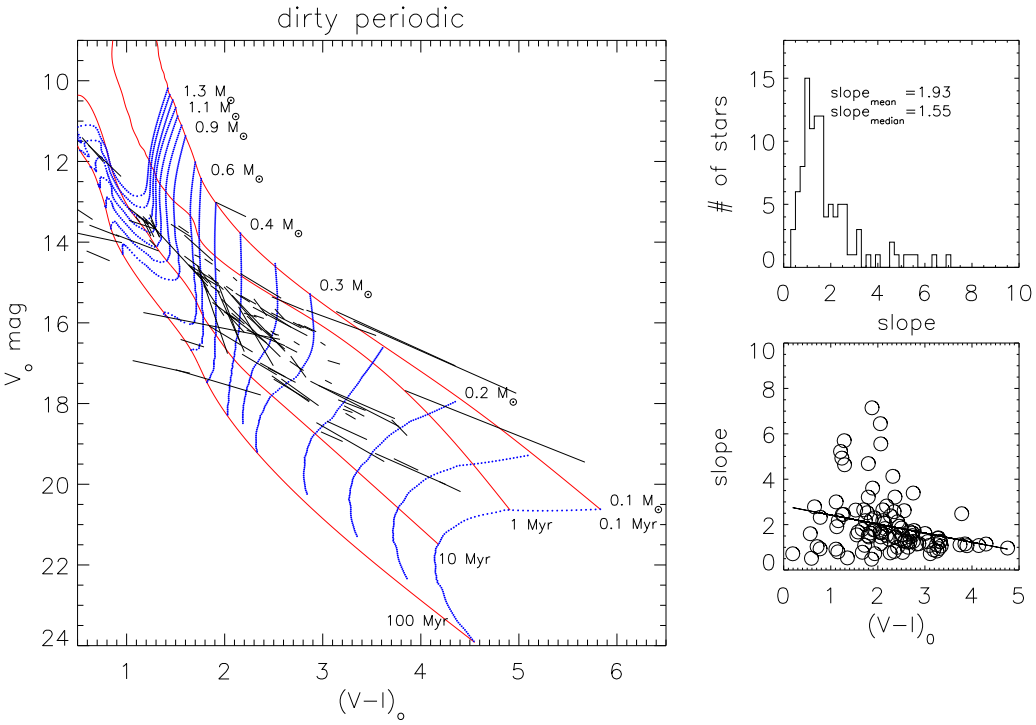

Figure 8. Same as in Fig. 5, but for I_0 versus $(V - I)_0$.

3.3 CMD for 'dirty' periodic light curves

We make an attempt to extend our analysis to the periodic 'dirty' sample. Owing to the large scatter of the phased light curves, we must take care to measure the brightest/faintest values and therefore the variability amplitude. In the Appendix, we provide a detailed discussion on the approaches to measure these quantities.

Once we have determined the amplitude of the periodic 'dirty' light curves, similarly to the 'clean' sample, we can build a CMD and use it to estimate the ages and masses corresponding to the brightest/bluest and faintest/reddest values. The results are plotted in Fig. 9, where we have selected only light curves where the magnitude and colour variations are correlated with a significance level larger than 90 per cent.

We note a few relevant differences. First, all stars have correlation coefficients $r < 0.90$. Second, a number of stars appear in regions of the CMD where no stars are expected, i.e. a few stars are either

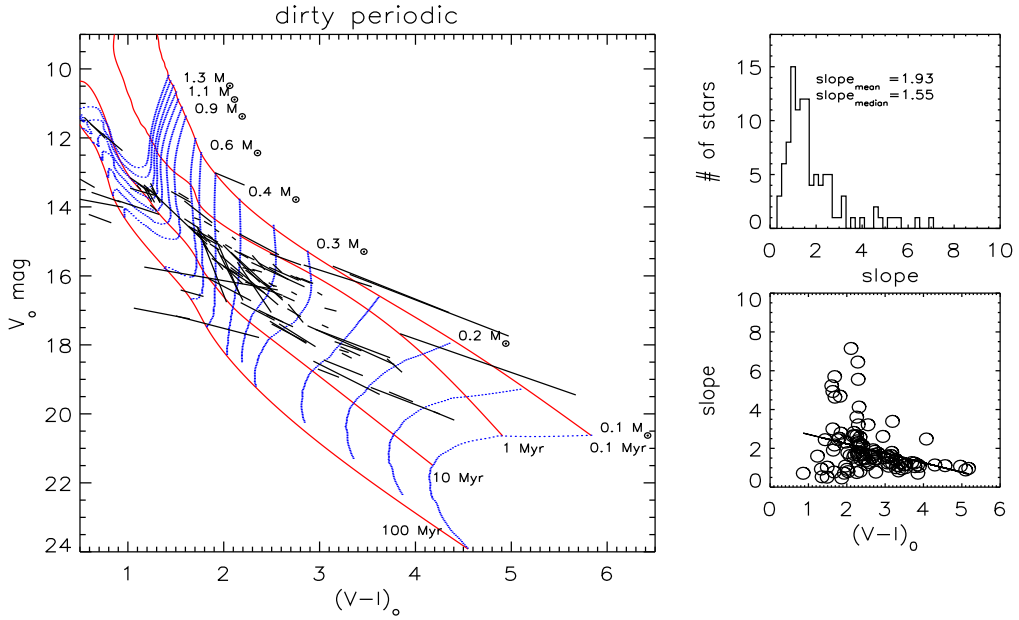

Figure 9. Left panel: V_0 versus $(V-I)_0$ diagram for the sample of 'dirty' light curves. Top right panel: distribution of slope of V_0 versus $(V-I)_0$ variations and (bottom right panel) versus $(V-I)_0$ colour.

too blue to be pre-main-sequence stars or too red to be older than about 1 Myr.

Finally, the average slope of the V_0 versus $(V-I)_0$ relation is smaller than in the 'clean' sample and has an average value $<\Delta V_0/\Delta(V-I)_0>=1.9$ (see top right panel of Fig. 9). This means that dirty periodic stars seem to exhibit either larger colour variations or smaller magnitude variations with respect to clean periodic stars. Since the average V_0 versus $(V-I)_0$ variation is less steep than the isochrones, the light curve faintest value therefore corresponds to a younger age than the brightest value when compared with the isochrones.

If we also consider in our analysis those light curves with correlation coefficients having a significance level smaller than 90 per cent, we find that the average slope is even smaller ($<\Delta V_0/\Delta(V-I)_0>=1.35$).

Similarly to the case of 'clean' light curves, in Fig. 6 and Fig. 7 we plot using dashed blue lines the distribution of ages and masses inferred from the CMD by comparing brightest/bluest and faintest/reddest values with isochrones and evolutionary mass tracks. We find 10 per cent of stars with age higher than 10 Myr and, excluding these stars, the average age is 3.5 and 3.1 Myr (from brightest and faintest magnitudes, respectively). The average difference between the age from brightest and faintest cases is still insignificant, although larger than in the case of 'clean' stars, i.e. −0.4 Myr against 0.1 Myr. However, the percentage of stars with age difference larger than 1 Myr has increased up to 20 per cent (with respect to 10 per cent for 'clean' stars). Therefore, when we consider the dominant variability component due to spots, together with the additional secondary component arising from either variable accretion or ARGD or stochastic events like microflares, then the average age appears to be greater (3.2 Myr against 2.7 Myr for clean periodic stars), as well as the percentage of stars with age estimate significantly affected by the variability increases up to 20 per cent. The average age is still older when we consider stars that still exhibit periodic light curves, but with no correlation (significance level smaller than 90 per cent) between magnitude and colour variations. Concerning mass, we find the average values 0.5 $M_\odot$ and 0.60 $M_\odot$ from brightest/bluest magnitude and faintest/reddest magnitudes, respectively, and an average difference of 0.04 $M_\odot$. Again, these differences are smaller than the precision associated with our mass determination.

3.4 CMD for dirty non-periodic stars

We consider now the sample consisting of non-periodic stars, the light curves of which can be assimilated to 'dirty' light curves. In Fig. 10, we plot the colour–magnitude diagram as well as the distribution of slopes and their trend with $(V-I)_0$ colour, as done in the previous cases. We see that the average slope of V_0 versus $(V-I)_0$ is $<\Delta V_0/\Delta(V-I)_0>=1.48$, similar to that inferred for 'dirty' stars with uncorrelated colour/magnitude variations. In Fig. 6, we plot the distribution of inferred ages. Excluding stars older than 10 Myr, which now represent about 50 per cent of the sample, we find that the age from the brightest magnitude is 4.6 Myr, that from the faintest magnitudes is 3.9 Myr and their difference is now −0.7 mag.

Concerning the mass, we find average values of 0.6 $M_\odot$ and 0.65 $M_\odot$ from the brightest/bluest magnitude and faintest/reddest magnitudes, respectively, and an average difference of 0.05 $M_\odot$. Again, these differences are smaller than the precision associated with our mass determination. Based on the presented results, it seems that when we pass from stars exhibiting 'regular' photometric variability, i.e. only due to surface inhomogeneities, to stars exhibiting 'irregular' photometric variability, i.e. dominated by accretion/stochastic phenomena, then the average age increases, as well as the impact of variability on the age estimate of individual stars – ages from brightest magnitude values are greater than ages inferred from faintest magnitude values. We can conclude by stating that, assuming all members are coeval, irregular photometric variability makes the stars appear older, increasingly so at increasing levels of variability.

4 ROTATION + LONG-TERM VARIABILITY

The analysis carried out in the previous sections considers the seasonal variability effects on age and mass arising from rotational

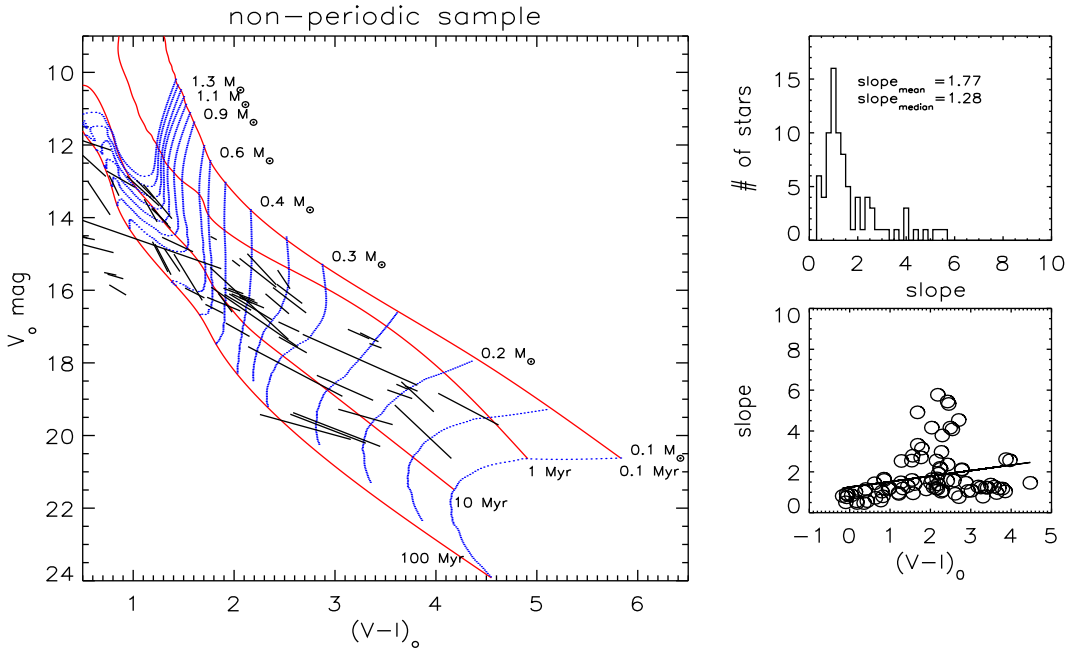

Figure 10. Left panel: V_0 versus $(V - I)_0$ diagram for the sample of non-periodic stars. Top right panel: distribution of slope of V_0 versus $(V - I)_0$ variations and (bottom right panel) versus $(V - I)_0$ colour.

modulation of active regions plus the additional random component not related to rotation. However, owing to ARGD and activity cycles, the brightest and faintest light-curve values of the same star can change from season to season. Therefore, in this section we have selected those clean stars with at least two observation seasons (up to five) and have plotted them in the CMD as segments connecting the brightest/bluest and faintest/reddest values ever observed. In this way, we consider the additional component related to long-term variability. However, at only 5 years, our longest time series generally samples only part of an activity cycle or long-term trend. Therefore, these estimates must also be regarded as lower limits on the impact of variability on age and mass determination.

We find that the average difference between ages derived from brightest and faintest values is about zero. However, the most relevant result is that the fraction of stars with differences larger that 1 Myr is now increased from 10 per cent (when only rotational variability was considered) to about 30 per cent.

5 SLOPE MODELLING

An important piece of information that we can derive from our multi-band monitoring is the dependence of magnitude versus colour variations, which in turn depends on the temperature contrast between the perturbed and surrounding unperturbed photosphere. Here, again we analyse the clean and dirty samples separately. In the top right panel of Fig. 5, we plot the distributions of slopes derived from the linear fit of V magnitude versus $V - I$ colour variations for the clean sample, whereas in the top right panels of Figs 9 and 10 we plot similar distributions for the dirty periodic and non-periodic samples, respectively. We note that the dirty periodic light curves, and to an even greater extent the non-periodic, tend to have smaller slopes, from 2.35 in the first sample to 1.77 in the last sample. In other words, when we consider scattered light curves, the amplitude of magnitude and colour variation tends to be similar, whereas in clean stars magnitude variations are larger than colour variations.

5.1 Correlation analysis

Magnitudes and colours of ONC stars are affected by both magnetic activity and star–disc interaction effects. In order to position our stars in colour–magnitude diagrams, we should use both unperturbed magnitudes and colours (or values properly corrected for the activity/accretion effects, at least). If only cool spots were present on the stellar surface, then the brightest magnitude and bluest colour could be assumed as presumably 'unspotted' values. This circumstance possibly applies to most WTTS, which are expected to lack accretion hot spots. However, also in WTTS, hot faculae of magnetic origin may be present, which can make the star bluer, meaning the brightest values do not correspond to an unspotted level. Moreover, in the case of binary systems with two components of different temperatures, when the more active and later-type star becomes fainter, owing to its variable activity, then the whole system becomes bluer (see e.g. Messina 2008). On the other hand, if only hot spots were present on the stellar surface, then the faintest magnitude and reddest colour could be assumed as 'unspotted' values (see Messina et al. 2016). Both regression and correlation analyses between magnitude and colours can allow us to understand better the patterns of colour variation of ONC stars and investigate the nature of surface inhomogeneities.

5.2 Model

We use the approach proposed by Dorren (1987) to simulate the amplitude of the V, R and I magnitudes and $V - R$, $R - I$ and $V - I$ colour variations arising from the difference of fluxes between opposite stellar hemispheres owing to the presence of surface temperature inhomogeneities. We note that our model assumes a two temperature photosphere, however, this is a simplified approach, the photosphere of T Tauri stars being likely more complex. The stellar fluxes were determined by using the NextGen atmosphere models of Hauschildt, Allard & Baron (1999) for solar metallicity and convolved with the passbands of the Bessel *UBVRI* system

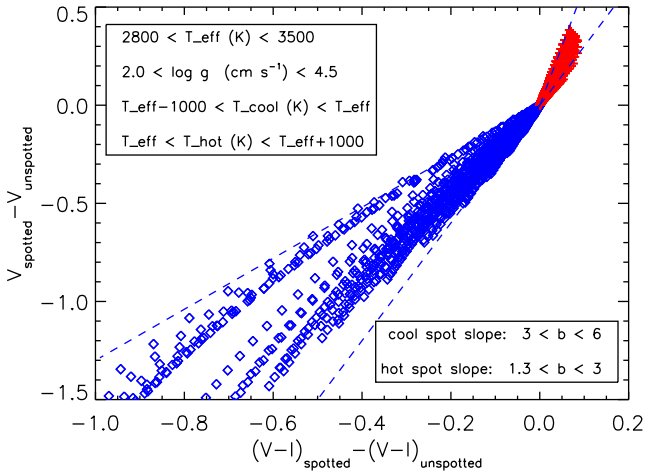

Figure 11. Model magnitude versus colour variations for a range of values of effective temperature, temperature contrast between perturbed and unperturbed photosphere and surface gravity.

(Bessel 1990). Limb-darkening coefficients, different for the unperturbed and the spotted photosphere, are taken from Diaz-Cordoves, Claret & Gimenez (1995). We have computed the model magnitude and color variations for a grid of values of temperature and covering fraction assuming a two temperature photosphere. More specifically, the hotter zone might be an accretion spot or faculae zone or it might just be the photospheric temperature. Similarly, the cool zone might be a region of magnetically inhibited convection or it might just be the photospheric temperature. The photospheric stellar magnitude and colors are computed over the effective temperature range of the majority of our targets ($2800 < T_{\rm eff}({\rm K}) < 3500$) and for a range of surface gravities ($2.0 < \log g < 4.5$). The covering fraction was varied from 0.0 (no temperature inhomogeneities) to 1.0 (stars fully covered by temperature inhomogeneities) with a 0.1 increment, whereas the temperature of the surface inhomogeneities was varied in the range $T_{\rm eff} - 1000 < T\,({\rm K}) < T_{\rm eff} + 1000$ (see, e.g., Berdyugina 2005) with a 100 K increment. In our modelling approach, gravity-darkening effects are neglected by considering that these effects tend to cancel out when computing the flux difference between opposite hemispheres. We have plotted in Fig. 11 the results of our modelling. We note that the amplitude of both magnitude and colour variations mostly depends on the filling factor of surface inhomogeneities, whereas the slopes of the magnitude versus colour variation mostly depend on the temperature contrast between such inhomogeneities and the unspotted photosphere. The presence of regions either cooler or hotter determines magnitude and colour variations, the slope Δ mag/Δ colour of which is positive in both cases: cooler regions make the star fainter and redder (see the solid red lines marked by crosses in the top right parts of Fig. 11), whereas hotter regions make the star brighter and bluer (both magnitude and colour variations are negative, as shown by the solid blue lines marked by diamonds in the bottom left parts of Fig. 11). We find that the families of slopes obtained by varying both the star's and the spot's parameters fall within a limited range of values. The most interesting result of our modeling is that slopes arising from the presence of only regions cooler ($3 < b < 5$) do not overlap with the slopes ($1.3 < b < 3$) arising from the presence of only regions hotter than the unperturbed photosphere. This allows us to use the V versus $V - I$ colour variation to investigate the nature of spots in our targets. In our simulations, we find that combinations of hot and cool spots simultaneously present on the same stellar hemisphere give rise to slope values close to zero or negative.

To compare the model results with observations, we have computed linear regression and correlation analysis and computed the relation slopes, their correlation coefficients and Pearson linear significance levels associated with the correlation coefficients for the V versus $V - I$, R versus $R - I$ and V versus $V - R$ magnitude–colour relations. The results are listed in Table 4, where we list the following information: internal identification number (id), observation season (seas), mean HJD ($\rm HJD_{mean}$), number of measurements in the I, R and V bands (N_I, N_R, N_V), slope of the V versus $V - I$ relation ($b_{V_{VI}}$) and correlation coefficient ($\rm r_{V_{VI}}$), slope of the R versus $R - I$ relation (b_{R_RI}) and correlation coefficient ($\rm r_{R\_RI}$), slope of the V versus $V - R$ relation (b_{V_VR}) and correlation coefficient ($\rm r_{V\_VR}$) and slope of the $R - I$ versus $V - R$ (b_{RI_VR}) and correlation coefficient ($\rm r_{RI\_VR}$). We listed and used in the following analysis only those values for which the correlation has a confidence level >95 per cent.

In Fig. 12, we plot the distribution of V versus $V - I$ slopes of all light curves. For a number of stars, we have at our disposal up to five values of slopes determined from data collected in five observation seasons. We verified that the slope distribution obtained by considering all light curves and the distribution obtained by using the mean slope for each star do not differ significantly. We also verified that no difference exists when we consider the whole sample of stars and a subsample of periodic stars. Finally, we opted to consider the whole sample of stars (periodic plus non-periodic) and the whole sample of light curves in order to have better statistics.

We find that about 6 per cent of light curves show a slope consistent with variability arising from only cool spots; 18 per cent of light curves show a slope with variability arising from only hot spots; whereas the majority (76 per cent) show slopes consistent with a variability arising from the presence of both cool and hot spots. We recall that periodic clean and periodic dirty stars have a mean slope in the range 1.5–2.2, whereas non-periodic stars, which are the majority, have smaller slopes. Moreover, bluer stars tend to have slopes steeper than redder stars.

This distribution provides us with an interesting interpretation of the cause of variability, i.e. stars with either only cool or only hot spots have inhomogeneity patterns sufficiently stable to produce periodic light variations. One such case is represented by the ONC member V1481 Ori (Messina et al. 2016), the photometric

Table 4. Summary of slopes and correlation coefficients of magnitude and colour variation among different photometric bands. The full table is available online.

[PMD2009]	Season	$\rm HJD_{mean}$	N_I	N_R	N_V	b_{V_VI}	r_{V_VI}	b_{R_RI}	r_{R_RI}	b_{V_VR}	r_{V_VR}	b_{RI_VR}	r_{RI_VR}
...	...	...	...	...	...	...	...	...	...	...	...	....	....
22	06–07	245 4443.8013	76	33	38	2.748	0.486	1.777	0.895	0.371	0.824	−0.581	0.57
25	06–07	245 4443.8013	77	34	43	0.996	0.984	0.908	0.708	0.982	0.994	−0.014	0.627
26	06–07	245 4443.8013	79	34	39	0.938	0.96	−0.530	0.665	0.966	0.994	0.226	0.64
...	...	...	...	...	...	...	...	...	...	...	...	....	....

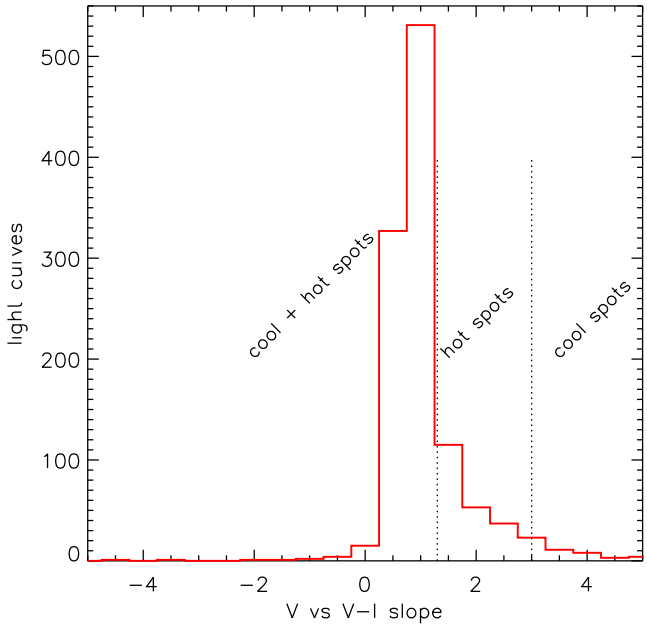

Figure 12. Distribution of V versus $V - I$ slopes for known WTTS and CTTS in our sample. The vertical dashed line indicates the region where, according to our model, the slope indicates the presence of only cool spots (slope > 3), only hotspots ($1 <$ slope < 3) and a combination of cool and hot spots (slope < 1).

variability of which is dominated by hot spots and the rotation period of which could be measured in 15 out 16 seasons. In contrast, when variability arises from the combined effect of hot and cool spots, the rotational modulation that results is very scattered and the stars are found to be non-periodic.

6 AGE VERSUS MAGNITUDE DISPERSION

We point out that the major aim of this study is not an absolute age determination of the ONC members under analysis, but rather the impact that the photometric variability may have on the inferred age. For this purpose, only one set of models accomplished this aim well.

We found that ages inferred by means of CMDs are not affected by photometric variability if stars exhibit a periodic photometric variability and the rotation phase magnitude dispersion is negligible with respect to the peak-to-peak light-curve amplitude ($R \geq 2.5$, the so-called 'clean periodic'). CMDs also still provide a reliable estimate of the age for periodic variables, the rotation phase magnitude dispersion of which becomes comparable to the peak-to-peak light-curve amplitude ($1 \leq R < 2.5$, the so called 'dirty periodic'). The inferred ages in these cases are slightly older and the number of outliers (stars with ages significantly older than the average) reaches 20 per cent. However, the majority of stars in our sample are non-periodic and ages inferred from CMDs become unreliable.

The information that we have obtained on photometric variability and use of magnitude–$T_{\rm eff}$ diagrams (to overcome uncertainties arising from the colour variability) can give us interesting information on the reality of the age spread among ONC members invoked by some authors (see e.g. Reggiani et al. 2011). In the following, we estimate the age of the ONC members using magnitude–$T_{\rm eff}$ diagrams, where the colour is replaced by the spectroscopically measured effective temperature. We focus on a subsample of stars with known reddening that comprises periodic and non-periodic members. In the left and right panels of Fig. 13, we plot the mean V_0 and I_0 magnitudes (averaged over the 5-yr time base) versus the effective temperatures taken from Hillenbrand (1997). The vertical bars indicate the observed maximum range of magnitude variation. Solid red and blue lines represent isochrones for ages from 0.1–100 Myr taken from Siess et al. (2000) and evolutionary mass tracks in the range 0.1 $M_\odot$–1.3 $M_\odot$. In Fig. 14, we plot the distributions of ages obtained considering the brightest/bluest magnitudes, faintest/reddest magnitudes and the difference between the highest and lowest ages for each star. We find that the average ONC age ranges from 1.7–3.3 Myr and that the photometric variability can produce an average age difference of 2.5 Myr in the V band and slightly larger in the I band.

To quantify the age dispersion, we measure the magnitude residuals with respect to a second-order polynomial fit in the magnitude–$T_{\rm eff}$ diagram. The distribution of the residuals is plotted in Fig. 15 and represented with a heavy solid red line. We compare this distribution with the distribution of the amplitudes of photometric variability overplotted with a heavy dashed blue line. A Gaussian fit to the distributions (dotted red and blues lines, respectively) is used to measure the standard deviations of both distributions. We find that the distribution of magnitude residuals with respect to the polynomial fit has standard deviation $\sigma = 0.70$ mag, which is comparable to the standard deviation $\sigma = 0.64$ mag of the distribution of variability amplitudes. These new results

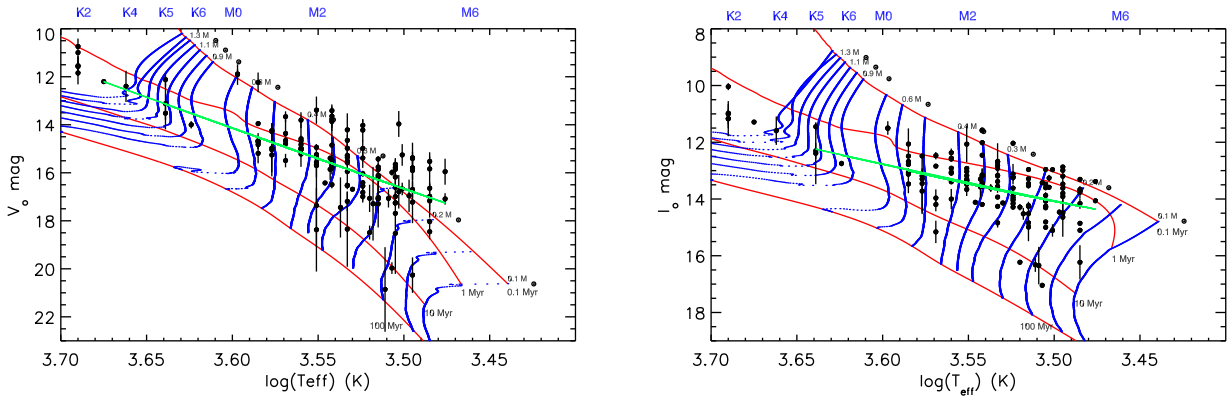

Figure 13. $T_{\rm eff} - V_0$ (left panel) and $T_{\rm eff} - I_0$ (right panel) diagrams of the ONC members under analysis for which the extinction is known. The black bullets represent the mean magnitudes (average magnitudes over a 5-yr long time series), the vertical bars their range of variation (brightest minus faintest magnitudes). Red solid lines and blue dotted lines represent theoretical isochrones and mass tracks, respectively, from Siess et al. (2000).

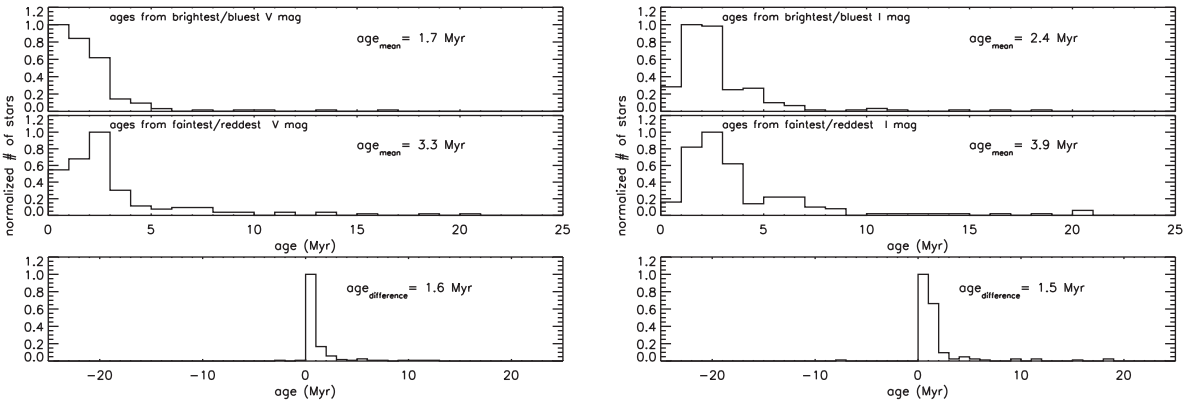

Figure 14. Comparison between the mean magnitude dispersion in the $T_{\rm eff} - V_0$ diagram and the amplitude of photometric variability (V band in left panel and I band in right panel). The magnitude dispersion is measured considering the residuals with respect to a second-order fit to the V_0 versus $T_{\rm eff}$ distribution. The amplitude of photometric variability is measured considering the brightest minus faintest magnitudes over a time range of 5 yr.

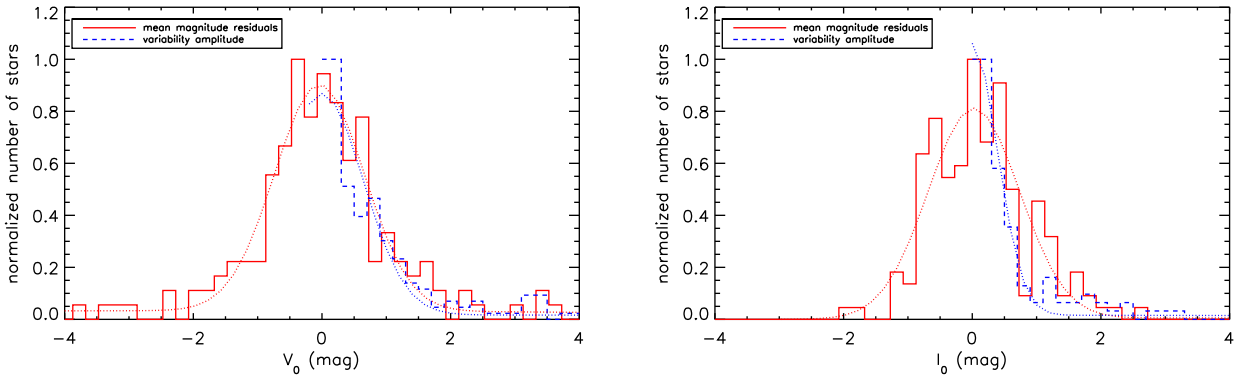

Figure 15. Comparison between the mean magnitude dispersion in the $T_{\rm eff} - V_0$ diagram and the amplitude of photometric variability (V band (left) and I band (right)). The magnitude dispersion is measured considering the residuals with respect to a second-order fit to the V_0 versus $T_{\rm eff}$ distribution. The amplitude of photometric variability is measured considering the brightest minus faintest magnitudes over a time range of 5 yr.

inferred from 5-yr V-band photometry supersede the conclusions by Reggiani et al. (2011) that observational uncertainties and variability cause a luminosity dispersion significantly smaller than the apparent age dispersion. In the case of the I magnitude, we find that the distributions of magnitude residuals and amplitudes have, respectively, standard deviations $\sigma = 0.71$ mag and $\sigma = 0.39$ mag.

This comparison in the I band indicates that the observed photometric variability can account for only a part (∼50 per cent) of the observed magnitude spread in the magnitude–$T_{\rm eff}$ diagrams. To account for the remaining 50 per cent, an intrinsic age spread among ONC members should be effectively invoked or, following Jeffries et al. (2011), a genuine radius dispersion among coeval members as a consequence of non-uniform accretion at early stages. In contrast, the comparison in the V band indicates that the photometric variability level is large enough to mask any age spread and, in principle, may be the unique cause of the observed magnitude spread.

As mentioned several times, our statistics on the variability provides only a lower limit, owing to the limited extension of the observation data base and insufficient time resolution for transient phenomena. However, as shown in Fig. 1, we do not expect that the variability amplitudes that we measured are significantly underestimated. The inferred age dispersion, if not real, must be imputed to some other effects beside the variability.

7 CONCLUSIONS

We have been monitoring a sample of 346 members of the ONC in the V, R and I bands for five consecutive years, from 2002–2003 to 2007–2008. Analysing the multi-band photometric time series, we detected magnitude and colour variability in all stars and with a wide range of amplitudes. We measured the magnitude and colour maximum and minimum values and the amplitude of variation of each star in each observation season and in the full 5-yr time series. We find that the amplitude of variability in the V band is on average a factor of two larger than in the I band. Moreover, the measured level of variability is found to increase as the monitoring time base extends. However, most of the range of variability is sampled after just 2–3 consecutive years of monitoring. The magnitude and colour maximum and minimum values were used to infer the mass and age of each star in colour–magnitude diagrams using isochrones and evolutionary mass tracks from the models of Siess et al. (2000). We found that stars showing periodic and very smooth rotational light variations undergo magnitude and colour variations with same slope as the theoretical isochrones. As a consequence, the variability does not affect their inferred mass and age. In contrast, stars showing periodic but very scattered rotational light variations or non-periodic stars undergo magnitude and colour variations with a slope smaller than that of theoretical isochrones and, consequently, appear older and more massive. Modelling the slope of the magnitude versus

colour variations, following the approach of Dorren (1987), we find that the use of V versus $V - I$ variations allows us to infer whether the photometric variability is caused by hot spots, cool spots, or a combination of both. We find that the majority of stars fall in the last category. Using magnitude–$T_{\rm eff}$ diagrams, in order to overcome the effects of colour variations, and the models of Siess et al. (2000), we find that the distribution of amplitudes of photometric variability in the V band has a dispersion comparable to the mean magnitude dispersion, which is attributed to age spread among the cluster members. Therefore, if we take for granted the age dispersion in the ONC, this is completely masked by the V-band variability. On the other hand, the amplitudes of variability in the I band have a dispersion a factor of two smaller than the I mean magnitude dispersion. Therefore, I-band variability takes account of only 50 per cent of the magnitude spread in the HR diagram. The remaining 50 per cent needs a different explanation and can support the invoked intrinsic age dispersion, which we find to be about 1.5 Myr.

ACKNOWLEDGEMENTS

Research on stellar activity at INAF–Catania Astrophysical Observatory is supported by MIUR (Ministero dell'Istruzione, dell'Universitá e della Ricerca). The work is based on data collected at the Indian Institute of Astrophysics (IIA). The extensive use of the SIMBAD and ADS data bases operated by the CDS centre, Strasbourg, France, is gratefully acknowledged. We thank the referee, Prof. W. Herbst, for valuable comments.

REFERENCES

Berdyugina S., 2005, Living Reviews in Solar Physics, 2, 62
Bessel M. S., 1990, PASP, 102, 1181
Da Rio N., Robberto M., Soderblom D. R., Panagia N., Hillenbrand L. A., Palla F., Stassun K. G., 2010, ApJ, 722, 1092
Diaz-Cordoves J., Claret A., Gimenez A., 1995, A&AS, 110, 329
Dorren J. D., 1987, ApJ, 320, 756
Grankin K. N., Melnikov S. Yu., Bouvier J., Herbst W., Shevchenko V. S., 2007, A&A, 461, 183
Grankin K. N., Bouvier J., Herbst W., Melnikov S. Yu., 2008, A&A, 479, 827
Hauschildt P. H., Allard F., Baron E., 1999, ApJ, 512, 377
Herbst W., Rhode K. L., Hillenbrand L. A., Curran G., 2000, AJ, 119, 261
Herbst W., Bailer-Jones C. A. L., Mundt R., Meisenheimer K., Wackermann R., 2002, A&A, 396, 513
Hillenbrand L. A., 1997, AJ, 113, 1733
Jeffries R. D., Littlefair S. P., Naylor T., Mayne N. J., 2011, MNRAS, 418, 1948
Messina S., Rodonó M., Guinan E. F., 2001, A&A, 366, 215
Messina S., Desidera S., Turatto M., Lanzafame A. C., Guinan E. F., 2010, A&A, 520, A15
Messina S., Desidera S., Lanzafame A. C., Turatto M., Guinan E. F., 2011, A&A, 532, A10
Messina S., 2008, A&A, 480, 495
Messina S., Rodonó M., Cutispoto G., 2004, Astron. Nachr., 325, 660
Messina S., Parihar P., Biazzo K., Lanza A. F., Distefano E., Melo C. H. F., Bradstreet D. H., Herbst W., 2016, MNRAS, 457, 3372
Oáh K. et al., 2009, A&A, 501, 703
Parihar P., Messina S., Distefano E., Shantikumar N. S., Medhi B. J., 2009, MNRAS, 400, 603
Reggiani M., Robberto M., Da Rio N., Meyer M. R., Soderblom D. R., Ricci L., 2011, A&A, 534, A83
Rodriguez-Ledesma M. V., Mundt R., Eisloeffel J., 2009, A&A, 502, 883
Siess L., Dufour E., Forestini M., 2000, A&A, 358, 593
Stassun K. G., Mathieu R. D., Mazeh T., Vrba F. J., 1999, AJ, 177, 2941

SUPPORTING INFORMATION

Supplementary data are available at *MNRAS* online.

Table 1. Summary of V-band photometry of ONC members.
Table 2. Summary of I-band photometry of ONC members.
Table 3. Summary of $V - I$ photometry of ONC members.
Table 4. Summary of slopes and correlation coefficients of magnitude and colour variation among different photometric bands.

Please note: Oxford University Press is not responsible for the content or functionality of any supporting materials supplied by the authors. Any queries (other than missing material) should be directed to the corresponding author for the article.

APPENDIX A: MEASUREMENT OF LIGHT-CURVE AMPLITUDE

As mentioned, to measure the amplitude of the clean periodic light curves, we use the amplitude of the sinusoidal fit. This secures no overestimation due to residual outliers. In the case of dirty periodic stars, the amplitude of the sinusoidal fit tends to underestimate the true light-curve amplitude. In this case, as well as in the case of non-periodic stars, to estimate the brightest and faintest magnitudes and the amplitude of variability we can follow two different approaches. One approach is to derive the relation between the light-curve amplitude and its root-mean-square (rms) using the clean stars sample. Then we apply the inferred transformation coefficients to estimate the light-curve amplitude of dirty stars from their rms. The results for different bands and colours are plotted in Fig. A1 and summarized in Table A1. In each panel, we report the correlation coefficient, its significance level according to the Person statistical test and the slope of a linear fit. The quantities are very well correlated and

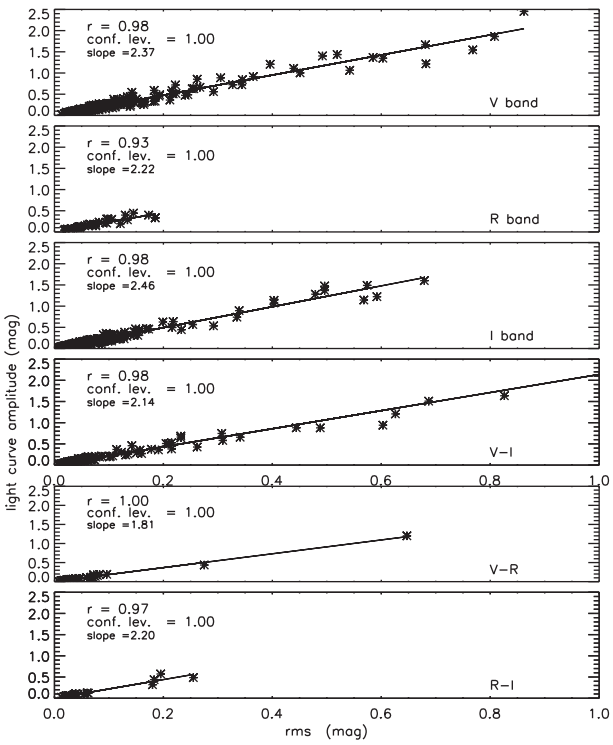

Figure A1. Distributions of light and colour curve amplitudes versus rms. Solid lines are linear fits. Labels report the correlation coefficient (r), the confidence level from the Pearson test and the slope of the linear fits.

Table A1. Average ratio between the amplitude and rms of light and colour curves.

Band	Amplitude/rms	# light curve
V	2.37 ± 0.03	235
R	2.22 ± 0.14	41
V	2.46 ± 0.02	350
$V-I$	2.14 ± 0.03	350
$V-R$	1.81 ± 0.03	27
$R-I$	2.30 ± 0.12	25

that provides us with the possibility of deriving the average light and colour curve amplitudes from the measurement of their rms for those stars with either unknown rotation period or light curves that are quite scattered ('dirty' periodic sample). To minimize the effect of outliers on the rms determination, we select only light curves with at least 30 measurements.

Another approach is to consider e.g. the 20 per cent brightest and 20 per cent faintest magnitudes of a 'dirty' light curve and to use their average values as measurement of the brightest and faintest magnitude. Both approaches can be tested in the case of clean light curves, which all have known amplitude, i.e. we can compare the distributions of amplitude derived from direct measurement of the amplitude of a sinusoidal fit, from transformation of rms into amplitude (first approach) and from averaging the extreme bands of the magnitude distribution (second approach).

We find that the amplitudes derived from both approaches differ by zero on average, with a dispersion of about 0.01 mag. As anticipated, we find that as the magnitude phase dispersion of the light curve increases (from clean to dirty), the amplitude of the sinusoidal fit becomes smaller than the amplitude derived from either the first or the second approach.

We also made a comparison between the distribution of the rms in clean and dirty samples to investigate further whether any significant difference exists. The confidence level that rms distributions of light curves in the 'dirty' and 'clean' samples come from the same parent distribution is computed with Kolmogorov–Smirnov (KS) tests. We find that it is larger than 99.9 per cent in the I band, 53 per cent in the R band and 13 per cent in the V band. Although the R-band distribution is based on 41 values, against the 243 values of the V band, its confidence level is higher. We suspect that the deviation of the 'dirty' distribution with respect to the 'clean', when we consider shorter wavelengths, arises from an increasing impact of variability phenomena not related to rotational modulation, rather than from poor statistics. A comparison between colour rms distributions reflects similar results: the $R-I$ colour has rms in the clean and dirty samples more similar than $V-R$ and $V-I$ ($\mathrm{KS}_{RI} = 83$ per cent, $\mathrm{KS}_{VI} = 35$ per cent, $\mathrm{KS}_{VR} = 21$ per cent). V-band amplitudes derived from the rms may be overestimated. The usefulness of deriving the amplitude from the rms consists of the possibility to investigate the impact of magnitude and colour variations in CMDs for a much larger stellar sample. We can verify that no dependence of the ratio on the star's brightness exists, since the photometric accuracy affects both the light-curve amplitude and the dispersion equally. To summarize, amplitudes of periodic clean light curves can be derived from sinusoid fits, rms and percentiles. Amplitudes of non-periodic or dirty light curves are better estimated from percentiles, since the sinusoid fit underestimates whereas the rms overestimates. To obtain a homogeneous estimate, we used the percentile in all light curves.

This paper has been typeset from a TEX/LATEX file prepared by the author.